Optimization of tumor treating fields using singular value decomposition and minimization of field anisotropy

Korshoej, Anders Rosendal; Sørensen, Jens Chr. Hedemann; Von Oettingen, Gorm; Poulsen, Frantz Rom; Thielscher, Axel

Published in:
Physics in Medicine and Biology

Link to article, DOI:
10.1088/1361-6560/aafe54

Publication date:
2019

Document Version
Publisher's PDF, also known as Version of record

Physics in Medicine & Biology

NOTE • **OPEN ACCESS**

Optimization of tumor treating fields using singular value decomposition and minimization of field anisotropy

To cite this article: Anders Rosendal Korshoej *et al* 2019 *Phys. Med. Biol.* **64** 04NT03

IOP Publishing Phys. Med. Biol. 64 (2019) 04NT03 (9pp) https://doi.org/10.1088/1361-6560/aafe54

Physics in Medicine & Biology

IPEM Institute of Physics and Engineering in Medicine

RECEIVED
3 September 2018

REVISED
17 December 2018

ACCEPTED FOR PUBLICATION
14 January 2019

PUBLISHED
8 February 2019

NOTE

Optimization of tumor treating fields using singular value decomposition and minimization of field anisotropy

Anders Rosendal Korshoej[1,2,3,6], Jens Chr. Hedemann Sørensen[1,2], Gorm von Oettingen[1,2], Frantz Rom Poulsen[3] and Axel Thielscher[4,5]

[1] Department of Neurosurgery, Aarhus University Hospital, Nørrebrogade 44, DK-8000 Aarhus C, Denmark
[2] Department of Clinical Medicine, Aarhus University, Palle Juul-Jensens Boulevard 82, DK-8200 Aarhus N, Denmark
[3] Department of Neurosurgery, Odense University Hospital, J.B. Winsløws vej 4, DK-5000 Odense, Denmark.
[4] Danish Research Centre for Magnetic Resonance, Centre for Functional and Diagnostic Imaging and Research, Copenhagen University Hospital Hvidovre, Kettegaards Allé 30, DK-2650 Hvidovre, Denmark
[5] DTU Elektro, Danish Technical University, 348 Ørsteds Plads, DK-2800 Kgs. Lyngby, Denmark
[6] Author to whom any correspondence should be addressed.

E-mail: andekors@rm.dk

Keywords: glioblastoma, tumor treating fields, finite element methods, anisotropy, optimization, neuro-oncology

Abstract

Tumor treating fields (TTFields) are increasingly used to treat newly diagnosed and recurrent glioblastoma (GBM). Recently, the authors proposed a new and comprehensive method for efficacy estimation based on singular value decomposition of the sequential field distributions. The method accounts for all efficacy parameters known to affect anti-cancer efficacy of TTFields, i.e. intensity, exposure time, and spatial field correlation. In this paper, we describe a further development, which enables individual optimization of the TTFields activation cycle. The method calculates the optimal device settings to obtain a desired average field intensity in the tumor, while minimizing unwanted field correlation.

Finite element (FE) methods were used to estimate the electrical field distribution in the head. The computational head model was based on MRI data from a GBM patient. Sequential field vectors were post-processed using singular value decomposition. A linear transformation was applied to the resulting field matrix to reduce fractional anisotropy (FA) of the principal field components in the tumor.

Results were computed for four realistic transducer array layouts. The optimization method significantly reduced FA and maintained the average field intensity in the tumor. The algorithm produced linear gain factors to be applied to the transducer array pairs producing the sequential fields. FA minimization was associated with an increase in total current delivered through the head during a activation cycle. Minimized FA can be obtained for an unchanged total current level, albeit with a reduction in average field intensity.

We present an algorithm for optimization of the TTFields activation cycle settings. The method can be used to minimize the spatial correlation between sequential TTFields, while adjusting the total current level and mean field intensity to a desired level. Future studies are needed to validate clinical impact and assess sensitivity towards model parameters.

Introduction

TTFields are intermediate frequency (100–300 kHz) alternating fields, which disrupt cancer growth. The treatment has proven effective against glioblastoma (GBM) (Stupp *et al* 2012, 2017, Mun *et al* 2018) and is currently being tried for multiple other solid tumors (Mun *et al* 2018). TTFields are induced by two current sources each connected a pair of 3 × 3 transducer arrays placed on the patient's scalp (Trusheim *et al* 2017). The sources are activated in sequence using a 50% activation cycle of 2 s total duration, i.e. each transducer pair is activated for 1 s followed by a 1 s 'off' period. When one pair is active the other is inactive and vice versa, i.e.

each pair is activated in a 'square waveform' pattern. During activation, the individual sources deliver sinusoidal field waveforms at 200 kHz (for GBM). The induced fields are applied in approximately orthogonal directions based on a perpendicular layout of the two array pairs. The therapeutic efficacy of TTFields depends on the induced field intensity as well as the exposure time and the direction of the sequential fields relative to each other (Kirson *et al* 2004). Specifically, the growth rate of cancer cell cultures has been shown to decrease with increasing intensity and exposure-time of TTFields (Kirson *et al* 2004). Similarly, a recent study showed that the overall survival of GBM patients treated with TTFields correlated positively with the cumulative TTFields exposure, calculated as the average field intensity over time (Urman *et al* 2017). TTFields has also been shown to preferentially disrupt mitosis for cells dividing in the direction of the applied field (Kirson *et al* 2004, Wenger *et al* 2015a). This latter notion is supported by the *in vivo* results showing that two sequential and orthogonal fields increase the therapeutic efficacy by ≈20% compared to one constantly active field (Kirson *et al* 2007). This illustrates that the use of multiple field directions enables the distribution of the anti-cancer effect more evenly among cells dividing in different (random) directions thereby reducing the average tendency to differentially inhibit cells dividing in particular directions. Correspondingly, clinical TTFields therapy (Optune®, Novocure, Ltd.) uses two pairs of transducer arrays activated in even 50% activation cycles, as explained above. The two corresponding fields cover two spatial directions and thereby target a larger fraction of cells compared to one field alone, although three linearly independent fields (ideally orthogonal and of equal magnitude) would be required to obtain an unbiased distribution. In a clinical treatment setting, the transducer array layout is planned to maximize the intensity of TTFields in the tumor (Trusheim *et al* 2017). However, in a recent study, we demonstrated that the complex anatomy and conductivity distribution of the head gives rise to considerable unwanted spatial correlation of the induced fields indexed as fractional anisotropy (FA). FA is extensively used in diffusion tensor imaging (Basser and Pierpaoli 2011). In the context of TTFields, it is calculated from the principal component magnitudes and measures the fractional deviation of the induced fields from the isotropic condition in which the sequential TTFields are perfectly orthogonal and have equal magnitude. FA generally takes values between zero and one, with higher values representing unwanted field correlation, i.e. the average field over an activation cycle will tend to have a directional preference of activity. Using the FA index, we have demonstrated considerable unwanted field correlation in the tumor region even for layouts planned to maximize treatment efficacy (Korshoej and Thielscher 2018). This means that although the array layouts were planned to induce orthogonal (i.e. uncorrelated) sequential fields, the actual induced fields were in fact highly correlated (figure 1) to each other. This problem has previously been ignored in TTFields treatment and computational studies of TTFields potentially compromising or reducing the therapeutic efficacy.

In this study, we propose a computational method, which optimizes the activation cycle settings of TTFields to minimize unwanted spatial field correlation in any local region of a computational volume conductor model. The optimization method is based on a linear transformation and can be used for any particular array layout, any number of active fields, and any choice of desired average field intensity in the tumor. We provide modeling data validating the method's ability to decorrelate the induced fields for different layouts. The method may potentially be used in future embodiments of the TTFields technology to optimize the treatment efficacy for individual cancer patients.

Methods

Model preparation and electrical field calculations

The head model was created from MRI data obtained from a patient with left-sided parietal GBM (figure 2(A)). Written consent was obtained from the patient. The head model was segmented into six tissue types, namely, skin, skull, cerebrospinal fluid (CSF), gray matter (GM), white matter (WM) and tumor. The configuration of TTFields was equivalent to the Optune® technology, which is used for clinical treatment. Four different array layouts were investigated (figure 2(C)). The distribution of the induced electric field was calculated using a finite element (FE) approximation of Laplace's equation for the electric potential, $\nabla \cdot (\sigma \nabla \varphi) = 0$ (Miranda *et al* 2014, Korshoej *et al* 2016, 2017a, 2017b, Bomzon *et al* 2016, Lok *et al* 2017). This is valid at the low-to-intermediate frequencies of TTFields (e.g. 200 kHz), because the electromagnetic wavelength in the relevant tissues is much larger than the size of the head (Plonsey and Heppner 1967, Miranda *et al* 2014, Wenger *et al* 2015b). Furthermore, skin effect can be neglected at 200 kHz. The currents induced by TTFields are, therefore, mainly resistive (Ohmic) currents. Regarding the relationship between field frequency and cancer growth inhibition, we kindly refer the reader to Wenger *et al* (2015) and Kirson *et al* (2004). Finite element calculations were performed with SimNIBS (www.simnibs.org) (Windhoff *et al* 2013). We used Dirichlet boundary conditions with a fixed electric potential at each array (Saturnino *et al* 2015, Opitz *et al* 2015). Isotropic conductivity values were assumed for skin (0.25 S m^{-1}), skull (0.010 S m^{-1}) and CSF (1.625 S m^{-1}) (Gabriel *et al* 2009, Korshoej *et al* 2016). For GM, WM and tumor tissues, we assumed anisotropic conductivity tensors inferred from diffusion MRI data (Tuch *et al* 2001, Korshoej *et al* 2016). The electric field was calculated as the numerical gradient of the potential. We

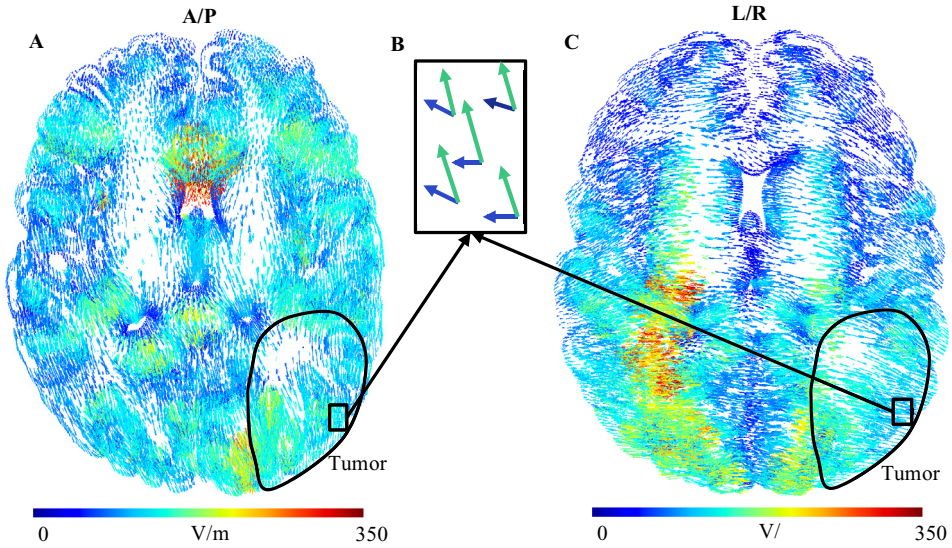

Figure 1. (A) and (C) Axial sections of the electric field distribution induced by the A/P and L/R array layouts, respectively. The field magnitude is indicated by the color bar (0–350 V m^{-1}) and a black line outlines the tumor. (B) Enlarged schematic view of the superimposed field vectors induced by the A/P (green) and L/R (blue) array layouts in a small region (five elements) of the tumor. The fields in each element display significant spatial correlation.

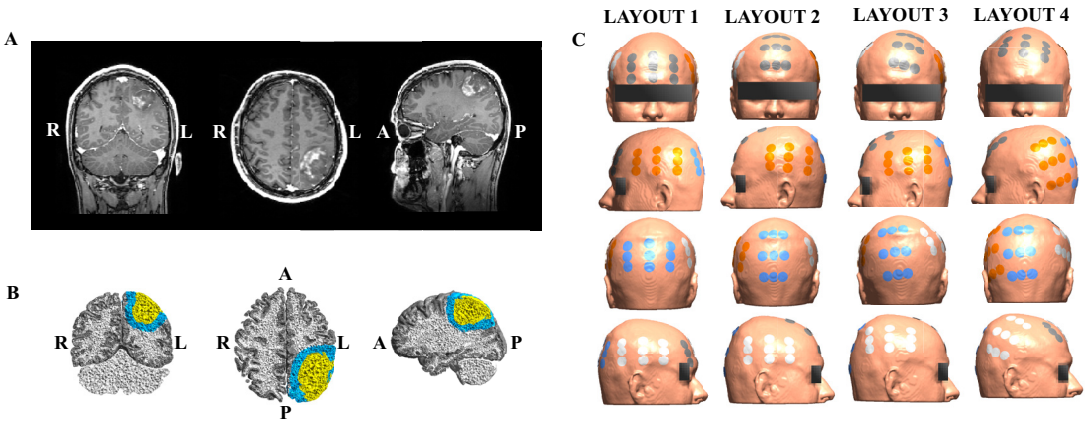

Figure 2. Head model used for finite element calculation of the electric field distribution. (A) Gadolinium enhanced T1 MRI data showing the patient's left parietal GBM. (B) Tetrahedral volume mesh reconstruction of MRI data segmented into different tissues. (C) Surface view of four different array layouts tested. The figure is adapted from Korshoej *et al* (2018).

calculated the current density using Ohm's law. The electric potentials, fields, and current densities were rescaled to obtain a peak-to-peak current amplitude of 1.8 A for each array pair. Further details about the head model generation and electric field calculation can be found in Korshoej *et al* (2016, 2017a, 2018) and Wenger *et al* (2018).

Estimation of average intensity and field correlation using singular value decomposition

For each finite element we defined the *field matrix*ε with the transposed sequential field vectors $\boldsymbol{E}_i$ in each row:

$$\varepsilon = \begin{bmatrix} \boldsymbol{E}_1^T \\ \vdots \\ \boldsymbol{E}_n^T \end{bmatrix} \epsilon \, \mathbb{R}^{n\times 3}. \tag{1}$$

In addition, we defined the *relative activation time* α_i of $\boldsymbol{E}_i$ as

$$0 < \alpha_i = \frac{t_i}{\sum_{j=1}^{n} t_j} < 1, \tag{2}$$

where $\boldsymbol{t}_i \geqslant \boldsymbol{0}$ is the 'on-time' of $\boldsymbol{E}_i$ during the activation-cycle ($\alpha_1 = \alpha_2 = \frac{1}{2}$ for Optune®, i.e. a 50% activation cycle). In this context, it is important to appreciate, that the notion of activation cycle in this context refers to the

pattern of field source activation and not the duty-cycle of the 200 kHz sinusoidal signal induced by the source. We used $\boldsymbol{A}\epsilon\mathbb{R}^{n\times n}$ as the diagonal activation time matrix with entries $a_{ii} = \sqrt{\alpha_i}$ and define an 'activation-time-weighted' electric field matrix

$$\boldsymbol{P} = \boldsymbol{A}\boldsymbol{\varepsilon}\epsilon\mathbb{R}^{n\times 3}. \tag{3}$$

We performed a singular value decomposition (SVD) of $\boldsymbol{P}$ to obtain a new representation of $\boldsymbol{P}$ defined by up to three principal components, i.e. orthonormal (uncorrelated) basis vectors collected in the matrix $\boldsymbol{W}\epsilon\mathbb{R}^{3\times 3}$:

$$\boldsymbol{P} = \boldsymbol{U}\boldsymbol{\Sigma}\boldsymbol{W}^T\epsilon\mathbb{R}^{n\times 3}. \tag{4}$$

The matrix $\boldsymbol{\Sigma}\epsilon\mathbb{R}^{n\times 3}$ contains the singular values $\sigma_k, k \leqslant 3$, i.e. the magnitudes of the principal components.

We defined the average intensity of TTFields in each element as the Frobenius norm of $\boldsymbol{P}$, i.e.

$$E_{avr} = \|\boldsymbol{P}\|_{\boldsymbol{F}} = \sqrt{\sum_{i=1}^{n} \alpha_i \boldsymbol{E}_i^2} = \sqrt{\sum_{k=1}^{3} \sigma_k^2}. \tag{5}$$

Thus, the average field was calculated as the square root of the activation-time weighted energy contributions from each field. The field correlation was estimated as the fractional anisotropy (FA) (Basser and Pierpaoli 2011), i.e.

$$FA = \sqrt{1/2}\frac{\sqrt{(\sigma_1-\sigma_2)^2+(\sigma_2-\sigma_3)^2+(\sigma_3-\sigma_1)^2}}{\sqrt{\sigma_1^2+\sigma_2^2+\sigma_3^2}}. \tag{6}$$

FA estimates the fractional deviation of $\boldsymbol{P}$ from the isotropic condition with orthogonal fields of equal intensity. In situations with <3 singular values the missing values were defined to be zero.

For a more detailed discussion of the above derivations and definitions, the reader is kindly referred to Korshoej and Thielscher (2018). Figure 3 shows a schematic illustration of the calculation steps.

Optimizing the activation cycle of TTFields to minimize the fractional anisotropy

The principle component approach allows for optimization of the activation cycle such that FA can be minimized at a predefined average intensity for any array layout and in any region of interest. This can be done by applying the following linear transformation to $\boldsymbol{P}$:

$$\boldsymbol{Q} = \boldsymbol{U}s\boldsymbol{I}_{nx3}\boldsymbol{\Sigma}^{+}\boldsymbol{U}^T\epsilon\mathbb{R}^{nxn}. \tag{7}$$

Here $s > 0$ is the desired isotropic singular value, $\boldsymbol{I}_{nx3}\epsilon\mathbb{R}^{nx3}$ is the truncated identity matrix and $\boldsymbol{\Sigma}^{+}\epsilon\mathbb{R}^{3xn}$ the pseudoinverse of $\boldsymbol{\Sigma}$. In the following, we will refer to $\boldsymbol{Q}$ as the *optimization matrix* and we note that $\boldsymbol{Q}$ is symmetric. We see that the transformed field matrix $\boldsymbol{G}$ is given by

$$\boldsymbol{G} = \boldsymbol{Q}\boldsymbol{P} = \boldsymbol{U}s\boldsymbol{I}_{nx3}\boldsymbol{\Sigma}^{+}\boldsymbol{U}^T\boldsymbol{U}\boldsymbol{\Sigma}\boldsymbol{W}^T = \boldsymbol{U}s\boldsymbol{I}_{nx3}\boldsymbol{W}^T, \tag{8}$$

which is clearly isotropic with two non-zero singular values equal to s as desired. Furthermore, $\boldsymbol{G}^T = \boldsymbol{P}^T\boldsymbol{Q}^T = \boldsymbol{\varepsilon}^T\boldsymbol{A}\boldsymbol{Q}^T$, so we may think of the column vectors of $\boldsymbol{G}^T$ as linear combinations of the original field vectors, in which the weighting factors defined by the entries in $\boldsymbol{A}\boldsymbol{Q}^T$ tell us how each field should be scaled to obtain an average distribution with minimum FA, i.e. equal singular values. To see this we define $\boldsymbol{g}_j$ to be the jth row vector of $\boldsymbol{G}$ and thus $\boldsymbol{g}_j^T$ is the jth column vector of $\boldsymbol{G}^T$. Then, $\boldsymbol{g}_j^T = \sum_{i=1}^{n} q_{ji}a_{ii}\boldsymbol{E}_i$ and as expected we see that the scale factors $q_{ji}a_{ii}$ of each field $\boldsymbol{E}_i$ depend on both the corresponding activation time and the entries of the transformation matrix $\boldsymbol{Q}$. Since the field vectors scale linearly with current, the jth row vector $\boldsymbol{q}_j$ of $\boldsymbol{Q}$ may be considered a vector of relative gain factors q_{ji} applied in the jth activation period of the electrode pair inducing the corresponding field. This gain may be considered a scale factor for a_{ii} (activation time) or for the induced electric current, i.e. reduced anisotropy may be obtained by scaling current impressed by either layout or by scaling their relative activation times. To demonstrate how this linear transformation is able to significantly reduce unwanted FA of the time-weighted field distributions, we first need to define the region of interest (ROI) to which the optimization is applied. For a ROI comprising the finite elements $k = 1, \ldots, m$ we define the average optimization matrix $\hat{\boldsymbol{Q}}$ as the median of optimization matrices $\boldsymbol{Q}_k$ of all m elements in the ROI weighted by the relative volumes $\boldsymbol{v_k}$. If we consider the entries of $\hat{\boldsymbol{Q}}$ as containing scale factors for the induced electric current density, then the field distribution of the optimized (on average) activation cycle is given by $\boldsymbol{G} = \hat{\boldsymbol{Q}}\boldsymbol{P}$ for each element, because the electric field depends linearly on the current density.

Results

In the following, we will provide examples of activation cycle optimization using four different array layouts. In addition, we will choose the desired isotropic singular value s so that E_{avr} is maintained, i.e. we seek to derive scale

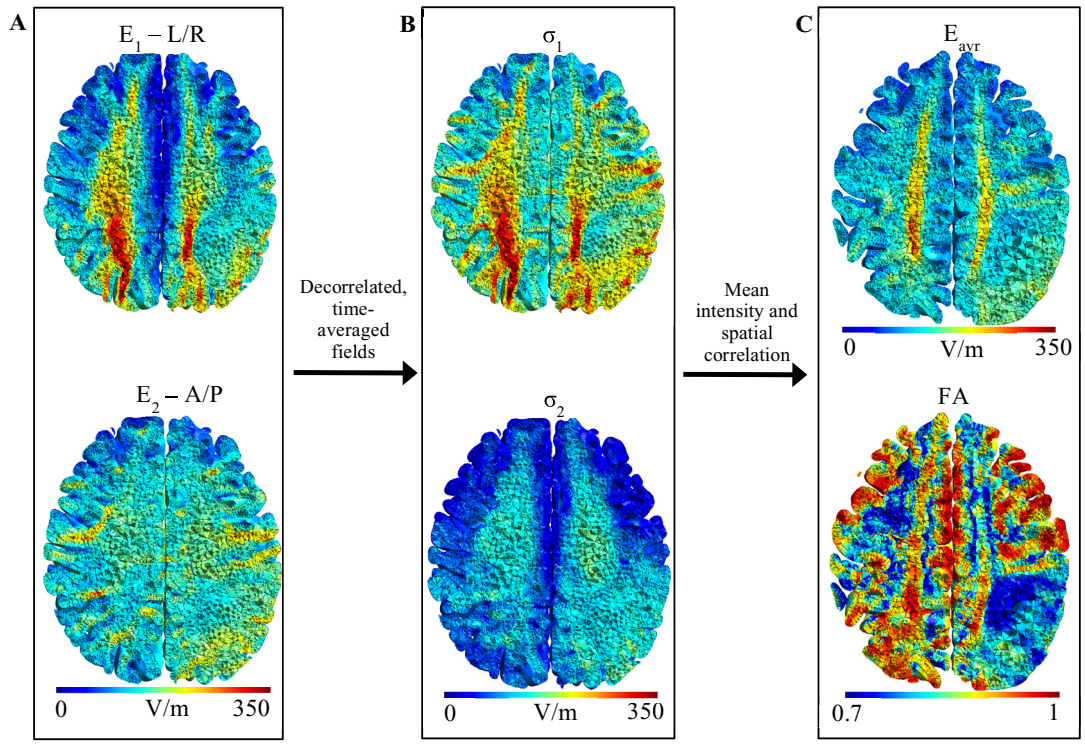

Figure 3. (A) Axial sections of the topografical intensity distributions (0–350 V m^{-1}) for the fields E_1 and E_2 induced by the L/R and A/P array layouts, respectively. (B) Topographical distributions of the minimum (σ_2, bottom) and maximum (σ_1, top) singular values (principal component magnitudes) after decomposition of the fields in each element. (C) Distributions of the mean intensity (E_{avr}, top) and spatial correlation (FA, bottom) calculated from the principal components of each element.

factors for current (or activation cycle period) settings of the TTFields device, which maintain the same average intensity, albeit with minimized FA in the tumor region. The objective is to distribute the energy isotropically in the span of the induced field vectors (rather than across all three dimensions of physical space), since we are using only two array layouts in accordance with the standard TTFields application. This corresponds to the best achievable activation cycle optimization possible with the number of active transducer arrays (i.e. fields). To achieve this we will set $s = \sqrt{\frac{\sum_{k=1}^{3}\sigma_k^2}{rank(\mathcal{E})}} = \frac{E_{avr}}{\sqrt{rank(\mathcal{E})}}$, so that the average intensity E_{avr} is maintained after activation cycle optimization. The potential impact of the optimization procedure is illustrated in figure 4, which shows a scatter plot of the singular values in each element of the field distribution in the tumor and the peritumoral regions before and after activation cycle optimization. The results were based on the field distribution induced by Layout 1 using standard current settings (1800 mA peak-to-peak) and relative activation times $\alpha_1 = \alpha_2 = \frac{1}{2}$. The figure confirms that the optimization procedure was able to reduce the difference between minimum and maximum singular values and hence reduce the FA in the ROI.

Figure 5 shows the cumulative distribution functions of E_{avr} (figures 5(A) and (C)) and FA (figures 5(B) and (D)) for four different layouts. Results are shown both before (solid) and after (stippled) activation cycle optimization. The optimization procedure maintains the E_{avr} distributions largely unaffected, while FA is reduced for all layouts. FA was particularly high for Layout 1, which also produced the highest median E_{avr}, and for this layout the optimization resulted in a pronounced reduction of FA. Thus the procedure was able to reduce FA and maintain mean intensity for all layouts, as expected, and the extent of FA reduction was higher for Layout 1, which had the most significant initial anisotropy.

The findings above are further illustrated in table 1, which gives the relative changes in the area under the curve (AUC) values for the distribution functions shown in figure 5 for all layouts and regions of interest. AUC was nearly unaffected (1.2%–2.9%) for E_{avr} in both the tumor and the peritumoral region, while the corresponding values for FA were considerably reduced (1.7%–43%).

The distribution of scale factors contained in the optimization matrix $\boldsymbol{Q}_k$ is shown in figure 6, using Layouts 1 to 4 and the tumor as the ROI. The values of $\hat{\boldsymbol{Q}}$ for the tumor were $\hat{\boldsymbol{Q}}_{Layout\ 1} = \begin{bmatrix} 1.03 & 0.06 \\ 0.06 & 1.06 \end{bmatrix}$, $\hat{\boldsymbol{Q}}_{Layout\ 2} = \begin{bmatrix} 1.02 & -0.03 \\ -0.03 & 1.06 \end{bmatrix}$, $\hat{\boldsymbol{Q}}_{Layout\ 3} = \begin{bmatrix} 1.05 & 0.06 \\ 0.06 & 1.04 \end{bmatrix}$, and $\hat{\boldsymbol{Q}}_{Layout\ 1} = \begin{bmatrix} 1.07 & -0.15 \\ -0.15 & 1.07 \end{bmatrix}$. It is evident that the

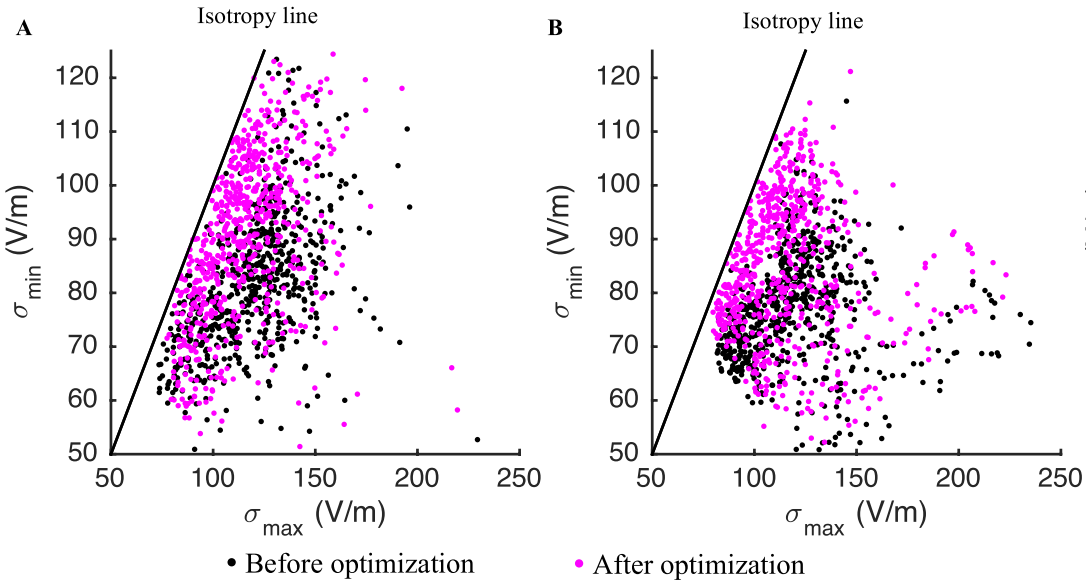

Figure 4. Scatterplot of the minimum (σ_{min}, 50–125 V m^{-1}) and maximum (σ_{max}, 50–250 V m^{-1}) singular values for each finite element in the tumor region (A) and peritumoral region (B). Results are shown before (black) and after (magenta) activation cycle optimization. The optimization procedure reduces the FA in the ROIs, i.e. it reduces the difference between the corresponding singular values and moves the points closer to the isotropy line (solid black).

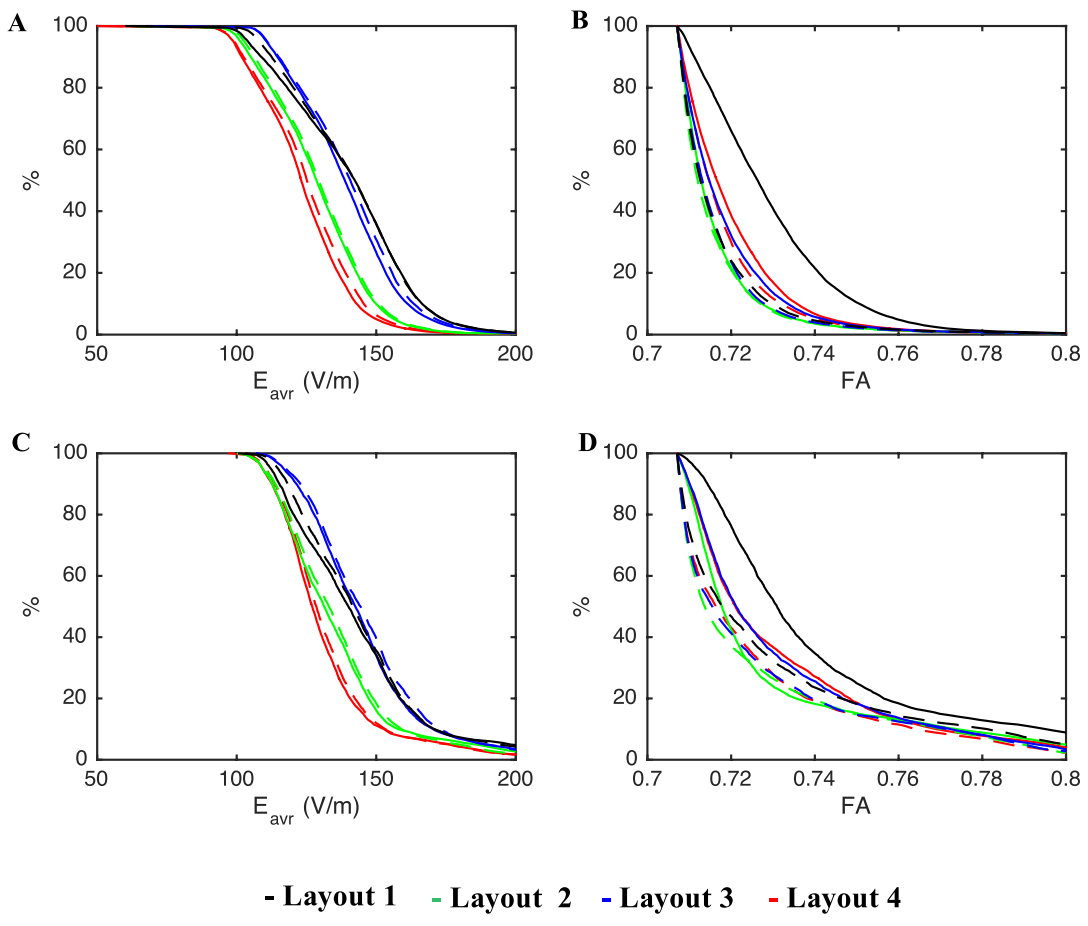

Figure 5. Cumulative distribution functions of E_{avr} (A) and (C) and FA (B) and (D). Results are shown for the tumor region (A) and (B) and peritumoral region (C) and (D). Results for the standard field distributions are shown in *solid*, while the distributions of the optimized activation cycle are shown in *stippled*. The activation cycle optimization reduces FA and maintains E_{avr} for all layouts.

Table 1. Relative change in AUC for E_{avr} and FA in the tumor and peritumoral regions for Layouts 1 to 4.

	Relative $\Delta AUC_{E_{avr}}$ tumor (%)	Relative ΔAUC_{FA} tumor (%)	Relative $\Delta AUC_{E_{avr}}$ peritumor (%)	Relative ΔAUC_{FA} peritumor (%)
Layout 1	1.20	−43.4	1.55	−38.4
Layout 2	1.46	−1.69	1.71	−6.9
Layout 3	1.52	−11.5	2.19	−13.4
Layout 4	2.93	−10.8	1.53	−15.8

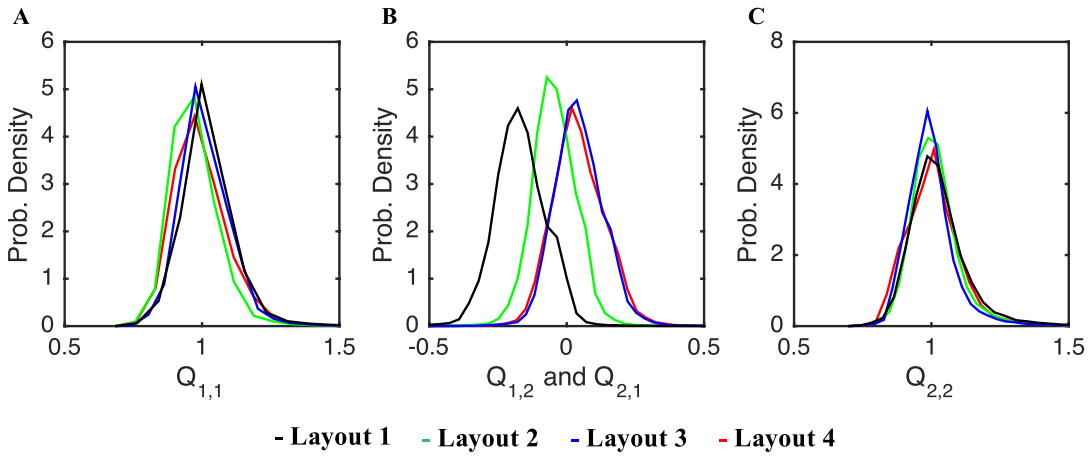

Figure 6. Probability density distributions of entries in the symmetric average optimization matrix. Panel (A) represents the matrix entry $Q_{1,1}$, panel (B) the identical diagonal entries $Q_{1,2}$ and $Q_{2,1}$, and panel (C) the entry $Q_{2,2}$.

absolute row sums of $\hat{\boldsymbol{Q}}$ are > 1, indicating that the induced current density (or activation cycle duration) required to maintain E_{avr} and minimize FA is higher than the default current settings. This can potentially be addressed by considering a normalized optimization matrix $\hat{\boldsymbol{Q}}_{norm}$ with entries $\hat{q}_{ij}^{norm} = \frac{\hat{q}_{ij}}{\sum_{j=1}^{rank(\varepsilon)} |\hat{q}_{ij}|}$, i.e. each entry normalized by the corresponding absolute row sum. This would ensure a constant total current density during each period of the activation cycle. The resulting field intensity would be lower than E_{avr} while FA would remain unchanged and minimized since the induced fields have the same direction but are scaled by the same factor. Consequently, the optimization process can be designed to consider the desired total current density, average field intensity and minimized FA in order to obtain an appropriate balance between these parameters.

Discussion

We have described a new method to optimize the activation cycle of TTFields for any given layout. The method enables minimization of unwanted spatial correlation (FA) of sequentially induced TTFields while maintaining the average field intensity at a desired level in a region of interest, or alternatively maintaining the total impressed current density at a particular level. The approach is based on a linear transformation of the distribution of principal field components, as derived by the authors in a separate study. The post-processing procedure is applied to calculated sequential field distributions in a volume conductor model. In this study, we have demonstrated that the algorithm robustly minimizes FA while maintaining the average field intensity for four different layouts.

The optimization method produces a matrix of linear scale factors representing either (1) electrical current gains applied to each sequential field during the activation cycle, or alternatively (2) scaling factors used to balance the duration of each period in the activation cycle. If the optimization matrix entries are interpreted as current gain factors, then the proposed method uses a balanced simultaneous activation of all array layouts to produce resulting field vectors, which on average are less spatially correlated in any small volume in a region of interest such as the tumor. This is contrary to the contemporary implementation TTFields, which uses strictly sequential fields. When the entries of the optimization matrix are interpreted as modifying factors for the activation cycle duration, the fields would still be applied sequentially, although each period would be scaled by the corresponding entry. When the optimization matrix is used to scale the current, the reduced FA and unchanged field intensity would imply a higher total current to be impressed by the system, compared to the default settings, which might potentially increase the risk of tissue heating. The user would therefore be required to personalize the activation cycle settings to obtain a desired balance between total current, average field and FA in the tumor. When the optimization matrix is used to scale the activation cycle periods, the induced peak current density

would be constant, however, a potential complication might be that FA minimization would imply longer relative activation time of the weaker field, while the stronger field would have a shorter relative activation time. Despite the fact that the weaker field is active for longer periods, the difference in activation time may potentially affect the tendency to develop skin rash underneath the transducer arrays, which is one of the more commonly observed complications to TTFields treatment. Also, it is important to note that the proposed optimization approach may be affected by non-linearities in the relationship between the field intensity and the anti-tumor efficacy. Until now, the intensity/response relationship has only been properly characterized for the field-range between 60 and 240 V m^{-1} *in vitro*, in which the relationship is approximately linear (Kirson *et al* 2004). However, it is possible that there exists a lower threshold for anti-tumor activity ($<$60 V m^{-1}), i.e. a field value below which no anti-tumor activity would be observed, which would imply that it would not be desirable to spend any time during the activation cycle at or below this level. Contrary, FA optimization would be more relevant in field ranges where the anti-tumor effect increases less than linear with increasing field strength. In those regimes, FA could potentially be reduced while largely maintaining the effectiveness of the array pair creating the peak field strengths. This could for instance be relevant if the anti-tumor activity would saturate at some higher field intensity (e.g. $>$240 V m^{-1}). In conclusion, future studies are required to establish the dose/response relationship of TTFields more accurately and it is necessary to incorporate information about field intensity and correlation in such studies.

Limitations and future perspectives

A key ability of the proposed method is to reduce unwanted spatial field correlation, which is known to influence the extent of cancer cell damage *in vitro*. However, future studies are needed to validate the clinical importance of FA as it was recently done for field intensity (Urman *et al* 2017). In addition, it is necessary to characterize the independent correlation of each parameter with clinical outcome to be able to predict the expected treatment efficacy and produce accurate optimization algorithms. Also, it would be valuable to characterize the sensitivity of the FA and E_{avr} estimates towards variations in model parameters (e.g. tissue conductivity) and tumor characteristics (e.g. morphology and location). Finally, it would be highly interesting to investigate potential performance limitations of the optimization algorithm, e.g. cases with very high FA in the region of interest. This might potentially be observed in cases with very high conductivity in the tumor or its vicinity due to shunting effects that would expectedly cause a locally inhomogeneous field distribution (Korshoej *et al* 2017a).

Acknowledgments

The work was supported by Lundbeckfonden (PI: Axel Thielscher, R118-A11308) and Novo Nordisk Fonden (PI: Axel Thielscher, NNF14OC0011413). Anders R Korshoej is the PI of a clinical trial (NCT02893137) partially funded by Novocure, which manufactures the Optune device for TTFields therapy.

ORCID iDs

Anders Rosendal Korshoej https://orcid.org/0000-0003-4285-8171
Gorm von Oettingen https://orcid.org/0000-0002-9707-3112
Frantz Rom Poulsen https://orcid.org/0000-0001-5715-6901
Axel Thielscher https://orcid.org/0000-0002-4752-5854

References

Basser P J and Pierpaoli C 2011 Microstructural and physiological features of tissues elucidated by quantitative-diffusion-tensor MRI *J. Magn. Reson.* **213** 560–70

Bomzon Z *et al* 2016 Using computational phantoms to improve delivery of Tumor Treating Fields (TTFields) to patients *2016 IEEE 38th Annual Int. Conf. of the Engineering in Medicine and Biology Society (EMBC)* (Orlando, FL, 16–20 August 2016) (https://doi/org/10.1109/EMBC.2016.7592208)

Gabriel C, Peyman A and Grant E 2009 Electrical conductivity of tissue at frequencies below 1 MHz *Phys. Med. Biol.* **54** 4863

Kirson E D *et al* 2004 Disruption of cancer cell replication by alternating electric fields *Cancer Res.* **64** 3288–95

Kirson E D *et al* 2007 Alternating electric fields arrest cell proliferation in animal tumor models and human brain tumors *Proc. Natl Acad. Sci. USA* **104** 10152–7

Korshoej A R and Thielscher A 2018 Estimating the intensity and anisotropy of tumor treating fields using singular value decomposition. Towards a more comprehensive estimation of anti-tumor efficacy *2018 40th Annual Int. Conf. of the IEEE Engineering in Medicine and Biology Society (EMBC) (Honolulu, HI, 18–21 July 2018)* pp 4897–900

Korshoej A R, Hansen F L, Mikic N, Thielscher A, von Oettingen G B and Sørensen J C H 2017b Exth-04. Guiding principles for predicting the distribution of tumor treating fields in a human brain: a computer modeling study investigating the impact of tumor position, conductivity distribution and tissue homogeneity *Neuro-Oncology* **19** vi73

Korshoej A R, Hansen F L, Mikic N, von Oettingen G, Sørensen J C H and Thielscher A 2018 Importance of electrode position for the distribution of tumor treating fields (TTFields) in a human brain. Identification of effective layouts through systematic analysis of array positions for multiple tumor locations *PLoS One* **13** e0201957

Korshoej A R, Hansen F L, Thielscher A, von Oettingen G B and Sørensen J C H 2017a Impact of tumor position, conductivity distribution and tissue homogeneity on the distribution of tumor treating fields in a human brain: a computer modeling study *PloS One* **12** e0179214

Korshoej A R, Saturnino G B, Rasmussen L K, von Oettingen G, Sørensen J C H and Thielscher A 2016 Enhancing predicted efficacy of tumor treating fields therapy of glioblastoma using targeted surgical craniectomy: a computer modeling study *PLoS One* **11** e0164051

Lok E, San P, Hua V, Phung M and Wong E T 2017 Analysis of physical characteristics of tumor treating fields for human glioblastoma *Cancer Med.* **6** 1286–300

Miranda P C, Mekonnen A, Salvador R and Basser P J 2014 Predicting the electric field distribution in the brain for the treatment of glioblastoma *Phys. Med. Biol.* **59** 4137

Mun E J, Babiker H M, Weinberg U, Kirson E D and Von Hoff D D 2018 Tumor treating fields: a fourth modality in cancer treatment *Clin. Cancer Res.* **24** 266–75

Opitz A, Paulus W, Will S, Antunes A and Thielscher A 2015 Determinants of the electric field during transcranial direct current stimulation *NeuroImage* **109** 140–50

Plonsey R and Heppner D B 1967 Considerations of quasi-stationarity in electrophysiological systems *Bull. Math. Biophys.* **29** 657–64

Saturnino G B, Antunes A and Thielscher A 2015 On the importance of electrode parameters for shaping electric field patterns generated by tDCS *NeuroImage* **120** 25–35

Stupp R *et al* 2012 NovoTTF-100A versus physician's choice chemotherapy in recurrent glioblastoma: a randomised phase III trial of a novel treatment modality *Eur. J. Cancer* **48** 2192–202

Stupp R *et al* 2017 Effect of tumor-treating fields plus maintenance temozolomide versus maintenance temozolomide alone on survival in patients with glioblastoma: a randomized clinical trial *JAMA* **318** 2306–16

Trusheim J *et al* 2017 A state-of-the-art review and guidelines for tumor treating fields treatment planning and patient follow-up in glioblastoma *CNS Oncol.* **6** 29–43

Tuch D S, Wedeen V J, Dale A M, George J S and Belliveau J W 2001 Conductivity tensor mapping of the human brain using diffusion tensor MRI *Proc. Natl Acad. Sci. USA* **98** 11697–701

Urman N *et al* 2017 Actr-91. Numerical simulations of ttfields distribution in patient models reveals a connection between field intensity and patient outcome *Neuro-Oncology* **19** vi20

Wenger C *et al* 2018 A review on tumor treating fields (TTFields): clinical implications inferred from computational modeling *IEEE Rev. Biomed. Eng.* **11** 195–207

Wenger C, Giladi M, Bomzon Z, Salvador R, Basser P J and Miranda P C 2015a Modeling tumor treating fields (TTFields) application in single cells during metaphase and telophase *2015 37th Annual Int. Conf. of the IEEE in Medicine and Biology Soceity (EMBC) (Milano, Italy, 25–29 August 2015)* (https://doi.org/10.1109/EMBC.2015.7319977)

Wenger C, Salvador R, Basser P J and Miranda P C 2015b The electric field distribution in the brain during TTFields therapy and its dependence on tissue dielectric properties and anatomy: a computational study *Phys. Med. Biol.* **60** 7339–57

Windhoff M, Opitz A and Thielscher A 2013 Electric field calculations in brain stimulation based on finite elements: an optimized processing pipeline for the generation and usage of accurate individual head models *Hum. Brain Mapp.* **34** 923–35